Supplementary Information

Sample Selection

We selected the final sample for the image analyses according to the following criteria: (1) Bad image coverage. We excluded the participants with imaging data that covered less than 90 precents of the group mask. The group mask was generated by extracting all brain regions that 90% of all participants' brain images covered. This discarded 15 participants. (2) Excessive head motion. Individuals with mean frame-wise displacement (FD) larger than 0.2 mm were excluded. Eighty-two individuals were discarded according to this criterion (3) Missing demographical data. Next, we removed participants without necessary demographical information (i.e., age, sex, education, and head motion), excluding 20 participants. This yielded a final sample containing 1574 MDD patients and 1308 HCs.

Preprocessing

The preprocessing of fMRI data was conducted using the toolbox for Data Processing & Analysis for Brain Imaging on Surface (DPABISurf)[1], which is based on fMRIPrep[2], FreeSurfer[3], ANTs[4], FSL[5], AFNI[6], SPM[7], PALM[8], dcm2niix[9], GNU Parallel[10], MATLAB (The MathWorks Inc., Natick, MA, US), Docker (https://docker.com) and DPABI[11]. The preprocessing pipeline included: i) discarding the initial 10 time points; ii) converting data into BIDS format[12]; iii) calling fMRIPrep 20.2.1 docker; iv) conducting anatomical data preprocessing as follows: correcting the T1-weighted image for intensity nonuniformity using N4BiasFieldCorrection[13]; the corrected T1-weighted image was then skull-stripped with ANTs[4]; fast (FSL 5.0.9)[14] was used to segment brain tissue into cerebrospinal fluid (CSF), white-matter (WM) and gray-matter (GM); recon -all (FreeSurfer 6.0.1)[3] was used to reconstruct brain surfaces; ANTs-derived brain masks and FreeSurfer-derived segmentations of the cortical GM were reconciled using a custom variation of the method of Mindboggle[15]; Nonlinear registration with antsRegistration (ANTs 2.3.3) was performed for the volume-based spatial normalization to one standard space (MNI152NLin2009cAsym)[16], using brain-extracted versions of both T1w reference and the T1w template. v) conducting functional data preprocessing as follows: generating a reference volume and its skull-stripped version using a custom methodology of fMRIPrep. The BOLD reference was then co-registered to the T1w reference using bbregister (FreeSurfer) which implements boundary-based registration[17]. Co-registration was configured with six degrees of freedom. Head-motion parameters with respect to the BOLD reference (transformation matrices, and six corresponding rotation and translation parameters) are estimated before any spatiotemporal filtering using mcflirt (FSL 5.0.9). BOLD runs were slice-time corrected using 3dTshift from AFNI 20160207 (RRID:SCR_005927)[6]. The BOLD time-series were resampled into standard space, generating a preprocessed BOLD run in MNI152NLin2009cAsym space; Confounding time-series were calculated based on the preprocessed BOLD series that are in the original space: framewise displacement (FD), DVARS and three region-wise global signals (extracted from the CSF, the WM, and the whole-brain masks). FD was computed using Jenkinson (relative root mean square displacement between affines) and referred to as $FD_{Jenkinson}$[5]. vi) Nuisance regression: The Friston 24-parameter model [18] was used to regress out head motion confounds. Additionally, mean framework displacement (FD) was used to address the residual effects of motion in group analyses[5]. Other sources of spurious variance (WM and CSF signals) were also removed from the data through linear regression to reduce respiratory and cardiac effects. Given the global signal regression (GSR) is an essential preprocessing step in identiying the TMS target[19], we performed preprocessing pipelines with and without GSR. Additionally, linear trends were included as a regressor to account for drifts in the blood oxygen level-dependent (BOLD) signal. vii) Finally, a bandpass temporal filter (0.01–0.1 Hz) was applied to the normalized functional images.

Harmonization of batch effects

ComBat models site-specific scaling factors by introducing terms for biological variables and scanners in a multivariate linear mixed effects regression. By employing empirical Bayesian criteria, it improves the estimation of studies with small sample sizes. ComBat assumes that the expected FC value can be modeled as a linear combination of batch effects and biological effects. Specifically, the error term in this model is modulated by additional site-specific scaling factors. Let y denote a given FC value:

$$y = \alpha + X^T\beta + \gamma + \delta\varepsilon \quad (1)$$

where $\boldsymbol{\alpha}$ denotes the constant term; X^T denotes the design matrix for covariates of interest (diagnosis, age, sex, education, head motion); $\boldsymbol{\beta}$ is a vector of regression coefficients corresponding to X; $\boldsymbol{\gamma}$ stands for addictive site effects (location parameter) while $\boldsymbol{\delta}$ represents multiplicative site effects (scale parameter). Accordingly, harmonized FC values were defined as:

$$y^{ComBat} = \frac{y - \hat{\alpha} - X^T\hat{\beta} - \hat{\gamma}}{\hat{\delta}} + \alpha + X^T\hat{\beta} \quad (2)$$

where $\hat{\delta}$ and $\hat{\gamma}$ stand for the empirical Bayesian estimates of $\boldsymbol{\delta}$ and $\boldsymbol{\gamma}$, respectively. y^{ComBat} was calculated with the “yw_Harmonization” function in DPABISurf (http://rfmri.org/DPABISurf). ComBat models biological and non-biological effects and algebraically removes the estimated additive and multiplicative batch effects.

Tables

Table S1. DIRECT site info, sample sizes and previous publications based on the shared data.

Serial Number	Sites (cohorts)	Principal investigators	Data organizer	N		Publications
				MDD	NC	
1	Faculty of Psychology, Southwest University	Jiang Qiu	Xin-Ran Wu	282	251	Cheng et al., 2016/ Ye et al., 2015[20,21]
2	Department of Psychiatry, The First Affiliated Hospital of Chongqing Medical University	Li Kuang	Qian Huang	151	63	Cao et al., 2016[22]
3	National Clinical Research Center for Mental Disorders (Peking University Sixth Hospital) & Key Laboratory of Mental Health, Ministry of Health (Peking University)	Tian-Mei Si	Yan-Kun Wu	20	20	Wang et al., 2013/Wang et al., 2015[23,24]
4	Mental Health Center, West China Hospital, Sichuan University	Tao Li	Hua Yu	34	30	Yang et al., 2015[25]
5	First Hospital of Shanxi Medical University	Ke-Rang Zhang	Ai-Xia Zhang	139	63	Li et al., 2014[26]
6	The Institute of Mental Health, Second Xiangya Hospital of Central South University	Zhe-Ning Liu	Yi-Cheng Long	67	106	Zeng et al., 2020/Tan et al., 2021/Long et al., 2020[27-29]
7	Affiliated Brain Hospital of Guangzhou Medical University	Li-Ping Cao	Jian-Shan Chen	24	30	Cheng et al., 2021[30]
8	The First Affiliated Hospital of Xi'an Jiaotong University, Xi'an Central Hospital	Jian Yang / Xiao-Ping Wu	Peng-Feng Sun	47	42	Wu et al., 2016[31]
9	Department of Psychosomatics and Psychiatry, Zhongda Hospital, School of Medicine, Southeast University	Yong-Gui Yuan	Xiao-Yun Liu	47	26	Hou et al., 2018/Hou et al., 2018[32,33]
10	Beijing Anding Hospital, Capital Medical University	Chuan-Yue Wang	Feng Li	85	70	Zheng et al., 2018/Liu et al., 2017[34,35]

11	Department of Neurology, Affiliated ZhongDa Hospital of Southeast University	Chun-Ming Xie	Can-Can He	116	68	Yuan et al., 2008[36]
12	The Second Xiangya Hospital of Central South University	Guang-Rong Xie	Xi-Long Cui	63	32	Yang et al., 2017[37]
13	Department of Clinical Psychology, Suzhou Suzhou Psychiatric Hospital, The Affiliated Guangji Hospital of Soochow University	Yan-Song Liu	Feng-Nan Jia	33	29	N/A
14	The First Affiliated Hospital of Anhui Medical University	Yong-Qiang Yu	Jia-Jia Zhu	139	147	Zhu et al., 2020/Zhao et al., 2022[38,39]
15	Xiangya 2nd Hospital, Central South University	Xiang Wang	Xin-Lei Ji	35	35	N/A
16	The First Affiliated Hospital of Jinan University	Ying Wang	Guan-Mao Chen	83	81	N/A
17	First Affiliated Hospital of Kunming Medical University	Xiu-Feng Xu / Yu-Qi Cheng	Zhao-Song Chu	47	50	He et al., 2022[40]
18	Huaxi MR Research Center, West China Hospital of Sichuan University	Qi-Yong Gong	Tao-Lin Chen	34	34	Chen et al., 2017[41]
19	The Second Xiangya Hospital of Central South University	Wen-Bin Guo/Jing-Ping Zhao	Xiao-Xiao Shan	32	32	Guo et al., 2014/Guo et al., 2018[42,43]
20	The First Affiliated Hospital, College of Medicine,Zhejiang University	Yang Hong	Tao Chen	20	20	N/A
21	Xijing Hospital	Hua-Ning Wang/Bao-Juan Li	Bao-Juan Li	63	56	N/A
22	West China Hospital, Sichuan University	Wei Zhang	Min-Lan Yuan	35	25	Xiao et al., 2021[44]
23	Shenzhen Mental Health Center, Shenzhen Kangning Hospital	Jian-ping Lu	Zhen-Peng Xue	64	31	N/A

				1660	1341	

Table S2. DIRECT image acquisition by site.

Serial Number	Scanner	Receive coil	TR (ms)	TE (ms)	Flip Angle (∘)	Thickness/gap (mm)	Slice number	Time points	Voxel size (mm)	FOV	Eyes open vs. closed	Slice order
1	Siemens Tim Trio 3T	12-channel	2000	30	90	3/1	32	242	3.44 × 3.44 × 4.00	220 × 220	closed	Interleaved Descending
2	GE Signa 3T	8-channel	2000	40	90	4/0	33	240	3.75 × 3.75 × 4.00	240 × 240	closed	Interleaved Ascending
3	Siemens Tim Trio 3T	32-channel	2000	30	90	4.0/0.8	30	210	3.28 × 3.28 × 4.80	210 × 210	closed	Interleaved Descending
4	Philips Achieva 3T TX	8-channal	2000	30	90	4.0/0	38	240	3.75 × 3.75 × 4.00	240 × 240	closed	Interleaved Ascending
5	Siemens Tim Trio 3T	32-channel	2000	30	90	3.00/1.52	32	212	3.75 × 3.75 × 4.52	240 × 240	closed	Interleaved Descending
6	Philips Gyroscan Achieva 3T	32-channel	2000	30	90	4/0	36	250	1.67 × 1.67 × 4.00	240 × 240	closed	Interleaved Ascending
7	Philips Achieva X-series 3T	8-channel	2000	30	90	4.0/0.6	33	240	3.44 × 3.44 × 4.60	220 × 220	closed	Interleaved Ascending
8	GE Excite 1.5T	16-channel	2500	35	90	4/0	36	150	4.00 × 4.00 × 4.00	256 × 256	closed	Interleaved Ascending

9	Siemens Verio 3T	12-channel	2000	25	90	4/0	36	240	3.75 × 3.75 × 4.00	240 × 240	closed	Interleaved Descending
10	Siemens Tim Trio 3T	32-channel	2000	30	90	3.5/0.7	33	240	3.12 × 3.12 × 4.20	200 × 200	closed	Interleaved Descending
11	Siemens Verio 3T	12-channel	2000	25	90	4/0	36	240	3.75 × 3.75 × 4.00	240 × 240	closed	Interleaved Descending
12	Siemens Tim Trio 3T	32-channel	2500	25	90	3.5/0	39	200	3.75 × 3.75 × 3.50	240 × 240	closed	Interleaved Descending
13	Siemens Skyra 3T	32-channel	2000	30	90	3.5/0	32	240	3.50 × 3.50 × 3.50	224 × 224	closed	Interleaved Ascending
14	GE Discovery MR750w 3T	24-channel	2000	30	90	3/1	35	185	3.40 × 3.40 × 4.00	220 × 220	closed	Interleaved Ascending
15	Siemens Skyra 3T X	32-channel	2000	30	90	4/0	36	240	3.44 × 3.44 × 4.00	220 × 220	open	Interleaved ascending
16	GE Discovery MR750 3T	8-channel	2000	25	90	3/1	35	200	3.75 × 3.75 × 4.00	240 × 240	closed	Interleaved Descending
17	Philips Achieva 3T	16-channel	4400	35	90	3	50	240	1.80 × 1.80 × 3.00	230 × 230	closed	Interleaved Ascending
18	GE Signa 3T	8-channel	2000	30	90	5/0	30	200	3.75 × 3.75 × 5.00	240 × 240	closed	Interleaved Ascending
19	Siemens Skyra 3T	32-channel	2000	30	90	4.0/0.6	33	240	3.40 × 3.40 × 4.60	220 × 220	closed	Interleaved Descending
20	GE Discovery 3T	16-channel	2000	30	90	3.2/0.4	43	200	3.40 × 3.40 × 3.40	220 × 220	closed	Interleaved Descending

21	GE Discovery MR750 3T	32-channel	2000	30	90	3.5/0	45	210	3.75 × 3.75 × 3.50	240 × 240	closed	Interleaved Ascending
22	Philips Achieva 3T	8-channel	2000	30	90	4/0	38	240	3.75 × 3.75 × 4.00	240 ×240	closed	Interleaved Descending
23	GE MR750 3T	8-channel	2000	30	90	3.2/0	43	240	3.4375 × 3.4375 × 3.2	220 × 220	closed	Interleaved Descending

Figures

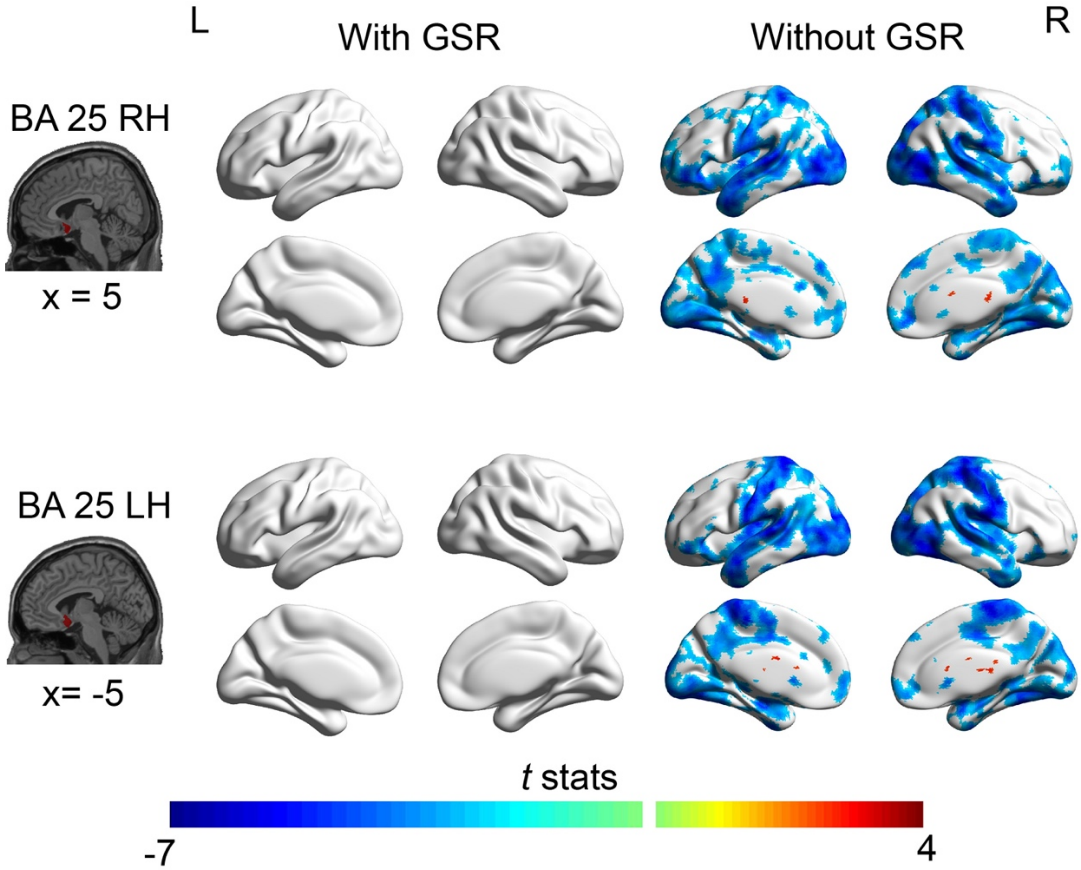

Figure S1. The case-control difference maps regarding the functional connectivity (FC) of the subgenual anterior cingulate cortex (sgACC) defined as an anatomical mask of Brodmann Area (BA) 25. Abbreviations: GSR, global signal regression; RH, right hemisphere; LH, left hemisphere.

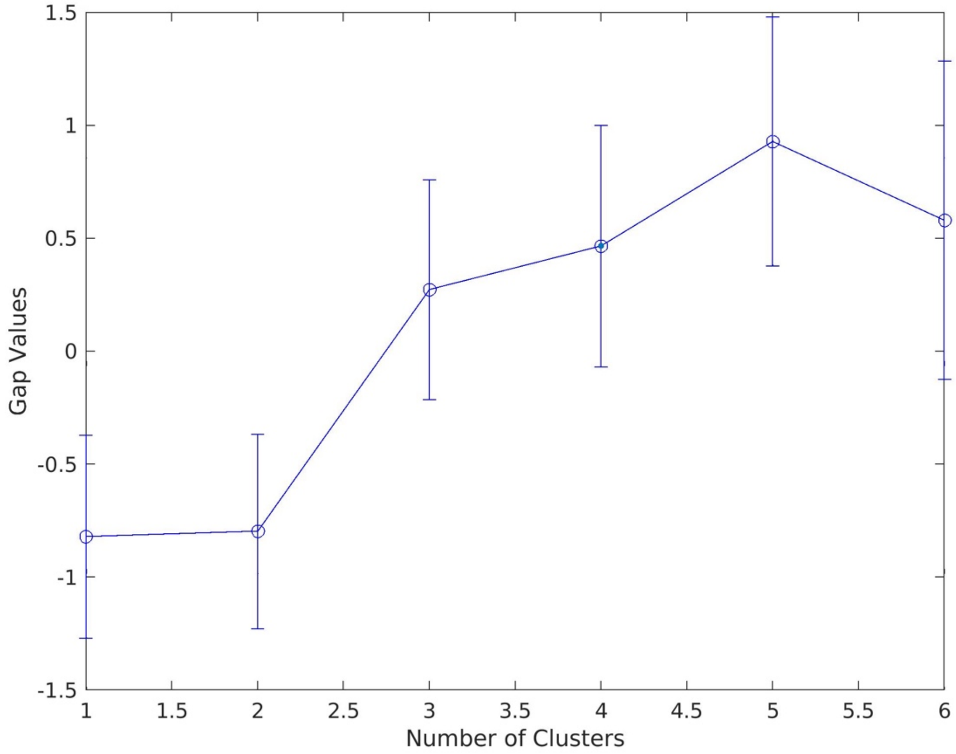

Figure S2. Gap statistics of different numbers of clusters in the hierarchical clustering of the group difference maps regarding functional connectivity (FC) of different left dorsal lateral prefrontal cortex (DLPFC) regions of interest (ROI).

References

1 Yan, C.-G., Wang, X.-D. & Lu, B. DPABISurf: data processing & analysis for brain imaging on surface. *Science Bulletin* (2021). https://doi.org:https://doi.org/10.1016/j.scib.2021.09.016

2 Esteban, O. *et al.* fMRIPrep: a robust preprocessing pipeline for functional MRI. *Nat Methods* **16**, 111-116 (2019). https://doi.org:10.1038/s41592-018-0235-4

3 Dale, A. M., Fischl, B. & Sereno, M. I. Cortical surface-based analysis. I. Segmentation and surface reconstruction. *Neuroimage* **9**, 179-194 (1999). https://doi.org:10.1006/nimg.1998.0395

4 Avants, B. B., Tustison, N. & Song, G. Advanced normalization tools (ANTS). *Insight j* **2**, 1-35 (2009).

5 Jenkinson, M., Bannister, P., Brady, M. & Smith, S. Improved Optimization for the Robust and Accurate Linear Registration and Motion Correction of Brain Images. *NeuroImage* **17**, 825-841 (2002). https://doi.org:http://dx.doi.org/10.1006/nimg.2002.1132

6 Cox, R. W. & Hyde, J. S. Software tools for analysis and visualization of fMRI data. *NMR Biomed* **10**, 171-178 (1997). https://doi.org:10.1002/(sici)1099-1492(199706/08)10:4/5<171::aid-nbm453>3.0.co;2-l

7 Ashburner, J. SPM: a history. *Neuroimage* **62**, 791-800 (2012). https://doi.org:10.1016/j.neuroimage.2011.10.025

8 Winkler, A. M., Ridgway, G. R., Webster, M. A., Smith, S. M. & Nichols, T. E. Permutation inference for the general linear model. *NeuroImage* **92**, 381-397 (2014). https://doi.org:http://dx.doi.org/10.1016/j.neuroimage.2014.01.060

9 Li, X., Morgan, P. S., Ashburner, J., Smith, J. & Rorden, C. The first step for neuroimaging data analysis: DICOM to NIfTI conversion. *J Neurosci Methods* **264**, 47-56 (2016). https://doi.org:10.1016/j.jneumeth.2016.03.001

10 Tange, O. Gnu parallel-the command-line power tool. *The USENIX Magazine* **36**, 42-47 (2011).

11 Yan, C.-G., Wang, X.-D., Zuo, X.-N. & Zang, Y.-F. DPABI: Data Processing & Analysis for (Resting-State) Brain Imaging. *Neuroinformatics* **14**, 339-351 (2016). https://doi.org:10.1007/s12021-016-9299-4

12 Gorgolewski, K. J. *et al.* The brain imaging data structure, a format for organizing and describing outputs of neuroimaging experiments. *Sci Data* **3**, 160044 (2016). https://doi.org:10.1038/sdata.2016.44

13 Tustison, N. J. *et al.* N4ITK: improved N3 bias correction. *IEEE Trans Med Imaging* **29**, 1310-1320 (2010). https://doi.org:10.1109/tmi.2010.2046908

14 Zhang, Y., Brady, M. & Smith, S. Segmentation of brain MR images through a hidden Markov random field model and the expectation-maximization algorithm. *IEEE Trans Med Imaging* **20**, 45-57 (2001). https://doi.org:10.1109/42.906424

15 Klein, A. *et al.* Mindboggling morphometry of human brains. *PLoS Comput Biol* **13**, e1005350 (2017). https://doi.org:10.1371/journal.pcbi.1005350

16 Fonov, V. S., Evans, A. C., McKinstry, R. C., Almli, C. R. & Collins, D. L. Unbiased

nonlinear average age-appropriate brain templates from birth to adulthood. *NeuroImage* **47** (2009). https://doi.org:https://doi.org/10.1016/S1053-8119(09)70884-5
17 Greve, D. N. & Fischl, B. Accurate and robust brain image alignment using boundary-based registration. *Neuroimage* **48**, 63-72 (2009). https://doi.org:10.1016/j.neuroimage.2009.06.060
18 Friston, K. J., Williams, S., Howard, R., Frackowiak, R. S. J. & Turner, R. Movement-Related effects in fMRI time-series. *Magnetic resonance in medicine* **35**, 346-355 (1996). https://doi.org:10.1002/mrm.1910350312
19 Fox, M. D., Liu, H. & Pascual-Leone, A. Identification of reproducible individualized targets for treatment of depression with TMS based on intrinsic connectivity. *Neuroimage* **66**, 151-160 (2013). https://doi.org:10.1016/j.neuroimage.2012.10.082
20 Cheng, W. *et al.* Medial reward and lateral non-reward orbitofrontal cortex circuits change in opposite directions in depression. *Brain* **139**, 3296-3309 (2016). https://doi.org:10.1093/brain/aww255
21 Ye, M. *et al.* Changes of Functional Brain Networks in Major Depressive Disorder: A Graph Theoretical Analysis of Resting-State fMRI. *PLoS One* **10**, e0133775 (2015). https://doi.org:10.1371/journal.pone.0133775
22 Cao, J. *et al.* Resting-state functional MRI of abnormal baseline brain activity in young depressed patients with and without suicidal behavior. *J Affect Disord* **205**, 252-263 (2016). https://doi.org:10.1016/j.jad.2016.07.002
23 Wang, L. *et al.* Interhemispheric functional connectivity and its relationships with clinical characteristics in major depressive disorder: a resting state fMRI study. *PLoS One* **8**, e60191 (2013). https://doi.org:10.1371/journal.pone.0060191
24 Wang, L. *et al.* The effects of antidepressant treatment on resting-state functional brain networks in patients with major depressive disorder. *Hum Brain Mapp* **36**, 768-778 (2015). https://doi.org:10.1002/hbm.22663
25 Yang, X. *et al.* Anatomical and functional brain abnormalities in unmedicated major depressive disorder. *Neuropsychiatr Dis Treat* **11**, 2415-2423 (2015). https://doi.org:10.2147/ndt.S93055
26 Li, H. J. *et al.* Surface-based regional homogeneity in first-episode, drug-naïve major depression: a resting-state FMRI study. *Biomed Res Int* **2014**, 374828 (2014). https://doi.org:10.1155/2014/374828
27 Zeng, C. *et al.* Salience-thalamic circuit uncouples in major depressive disorder, but not in bipolar depression. *J Affect Disord* **269**, 43-50 (2020). https://doi.org:10.1016/j.jad.2020.03.007
28 Tan, W. *et al.* Decreased integration of the frontoparietal network during a working memory task in major depressive disorder. *Aust N Z J Psychiatry* **55**, 577-587 (2021). https://doi.org:10.1177/0004867420978284
29 Long, Y. *et al.* Altered resting-state dynamic functional brain networks in major depressive disorder: Findings from the REST-meta-MDD consortium. *Neuroimage Clin* **26**, 102163 (2020). https://doi.org:10.1016/j.nicl.2020.102163
30 Cheng, X. *et al.* Alterations in resting-state global brain connectivity in bipolar I disorder patients with prior suicide attempt. *Bipolar disorders* **23**, 474-486 (2021).

https://doi.org:10.1111/bdi.13012
31 Wu, X. *et al.* Dysfunction of the cingulo-opercular network in first-episode medication-naive patients with major depressive disorder. *J Affect Disord* **200**, 275-283 (2016). https://doi.org:10.1016/j.jad.2016.04.046
32 Hou, Z. *et al.* Increased temporal variability of striatum region facilitating the early antidepressant response in patients with major depressive disorder. *Progress in neuro-psychopharmacology & biological psychiatry* **85**, 39-45 (2018). https://doi.org:10.1016/j.pnpbp.2018.03.026
33 Hou, Z. *et al.* Distinctive pretreatment features of bilateral nucleus accumbens networks predict early response to antidepressants in major depressive disorder. *Brain imaging and behavior* **12**, 1042-1052 (2018). https://doi.org:10.1007/s11682-017-9773-0
34 Zheng, H. *et al.* The dynamic characteristics of the anterior cingulate cortex in resting-state fMRI of patients with depression. *J Affect Disord* **227**, 391-397 (2018). https://doi.org:10.1016/j.jad.2017.11.026
35 Liu, Y. *et al.* Regional homogeneity associated with overgeneral autobiographical memory of first-episode treatment-naive patients with major depressive disorder in the orbitofrontal cortex: A resting-state fMRI study. *J Affect Disord* **209**, 163-168 (2017). https://doi.org:10.1016/j.jad.2016.11.044
36 Yuan, Y. *et al.* Abnormal neural activity in the patients with remitted geriatric depression: a resting-state functional magnetic resonance imaging study. *J Affect Disord* **111**, 145-152 (2008). https://doi.org:10.1016/j.jad.2008.02.016
37 Yang, X. H. *et al.* Anhedonia correlates with abnormal functional connectivity of the superior temporal gyrus and the caudate nucleus in patients with first-episode drug-naive major depressive disorder. *J Affect Disord* **218**, 284-290 (2017). https://doi.org:10.1016/j.jad.2017.04.053
38 Zhu, D. M. *et al.* Cerebellar-cerebral dynamic functional connectivity alterations in major depressive disorder. *J Affect Disord* **275**, 319-328 (2020). https://doi.org:10.1016/j.jad.2020.06.062
39 Zhao, W. *et al.* Brain function mediates the association between low vitamin D and neurocognitive status in female patients with major depressive disorder. *Psychol Med*, 1-14 (2022). https://doi.org:10.1017/s0033291722000708
40 He, M. *et al.* Identifying Changes of Brain Regional Homogeneity and Cingulo-Opercular Network Connectivity in First-Episode, Drug-Naïve Depressive Patients With Suicidal Ideation. *Front Neurosci* **16**, 856366 (2022). https://doi.org:10.3389/fnins.2022.856366
41 Chen, T. *et al.* Anomalous single-subject based morphological cortical networks in drug-naive, first-episode major depressive disorder. *Hum Brain Mapp* **38**, 2482-2494 (2017). https://doi.org:10.1002/hbm.23534
42 Guo, W. *et al.* Abnormal default-mode network homogeneity in first-episode, drug-naive major depressive disorder. *PLoS One* **9**, e91102 (2014). https://doi.org:10.1371/journal.pone.0091102
43 Guo, W. *et al.* Decreased interhemispheric coordination in the posterior default-mode network and visual regions as trait alterations in first-episode, drug-naive

major depressive disorder. *Brain imaging and behavior* **12**, 1251-1258 (2018). https://doi.org:10.1007/s11682-017-9794-8

44 Xiao, H. *et al.* Functional connectivity of the hippocampus in predicting early antidepressant efficacy in patients with major depressive disorder. *J Affect Disord* **291**, 315-321 (2021). https://doi.org:10.1016/j.jad.2021.05.013